JOURNAL OF AIRCRAFT
Vol. 39, No. 4, July–August 2002

Separation Control on a Cantilever Wing with a Self-Excited Vibrating Rod

Rong F. Huang* and Shih W. Mao†
National Taiwan University of Science and Technology, Taipei 106, Taiwan, Republic of China

The surface-flow characteristics and aerodynamic performance of a cantilever wing model subjected to the influence of a leading-edge control rod are studied in a wind tunnel. Circular rods of various materials and diameters installed at various distances from the leading edge of the wing are tested at low chord Reynolds numbers. Some selected small-diameter rods present a self-excited transverse vibration when they are placed very close to the leading edge. Through the surface oil-flow technique, the natural wing displays complex surface-flow patterns, which are commonly observed at a Reynolds-number range of 10^4–10^6. Under the action of rod vibration, turbulent boundary-layer behaviors usually found on a wing surface at large Reynolds numbers are observed. The separation resistance of boundary layer on the vibrating-rod controlled wing is remarkably larger than the natural and rod-wake disturbed wings. Measurements of aerodynamic loads using a PC-based force/moment sensing system show that the stall angle can be postponed by around 80%, the maximum lift-coefficient can be increased by about 20%, and the lift/drag ratio might be increased by approximately 50% at large angles of attack. The improvements of lift and stall angle of attack are closely related to the modulation of surface flow, which is caused by the vibration-induced transverse velocity fluctuations superimposed on the boundary layer. Details of the influences are discussed and illustrated.

Nomenclature

A	=	vibration amplitude of rod
b	=	span of wing, 30 cm
C_D	=	drag coefficient ($= D/qbc$)
C_L	=	lift coefficient ($= L/qbc$)
$C_{L\,\max}$	=	maximum lift coefficient prior to stall
$C_{L\,\max,o}$	=	maximum lift coefficient of natural wing
c	=	chord length of wing, 6 cm
D	=	drag force, measured by balance in freestream direction
f_s	=	nominal vibration frequency of rod
L	=	lift force, measured by balance in cross free stream direction
l	=	minimum distance between rod surface to leading edge of wing model
q	=	dynamic pressure of freestream ($= 0.5\rho_w u_w^2$)
Re_c	=	Reynolds number based on chord length of wing ($= u_w c/\nu_w$)
St_s	=	Strouhal number of rod vibration ($= f_s c/u_w$)
u_w	=	freestream velocity in wind-tunnel test section
x	=	streamwise coordinate, originated from leading edge of wing
y	=	spanwise coordinate, originated from leading edge of wing on root plane
α	=	angle of attack
α_{stall}	=	angle of attack at stall
$\alpha_{\text{stall},o}$	=	stall angle of attack of natural wing
ν_w	=	kinematic viscosity of air in test section of wind tunnel
ρ_w	=	density of air in test section of wind tunnel
ϕ	=	rod diameter

Received 8 December 2000; revision received 16 February 2002; accepted for publication 14 March 2002.

*Professor, Department of Mechanical Engineering, 43 Keelung Road, Section 4; rfhuang@mail.ntust.edu.tw. Senior Member AIAA.

†Graduate Student, Department of Mechanical Engineering, 43 Keelung Road, Section 4.

Introduction

IN the range $10^4 < Re_c < 10^6$ where flying animals, large model airplanes, man-carrying hang-gliders, human-powered aircraft, remotely piloted vehicles are categorized, many complicated phenomena take place within the boundary layer of the airfoils.[1–11] The laminar boundary layer, transition, separation, reattachment, separation bubble, etc. characterize the flows on the lifting surface in this range of Reynolds number. At low chord Reynolds numbers and angles of attack, the separation bubble generally extends over a large portion of the chord length and significantly changes the pressure distribution by tremendously altering the shape of the outer potential stream flow. The aerodynamic performance in this range of Reynolds number is usually low because of the characteristics of surface flows.

A variety of passive and active techniques can be used to change the complex surface flows on the airfoils and thus the aerodynamic performance in the range $10^4 < Re_c < 10^6$. Gad-el-Hak[3,12] has made a detailed review on the flow phenomena as well as the methods and mechanisms of flow control. Most of the methods currently used are primarily aimed to prevent the boundary layer separating from wing surface. For instance, tripping[13,14] and shaping[15] are among the simplest passive methods, whereas the fence,[16,17] spoiler-like flap,[18] wall transpiration,[19] heat transfer,[20] acoustic excitation,[21–23] etc. are examples of active control methods to ensure flow attachment beyond a critical angle of attack and thus, an improved performance. The ultimate goal of all of these methods is to improve the airfoil's performance by increasing the stall angle and/or lift-to-drag ratio.

When using the acoustic excitation, Zaman et al.[22] found that the most effective separation control is achieved at frequencies in which the acoustic standing waves that form in the test section induce transverse velocity fluctuations (rather than pressure fluctuations) in the vicinity of the airfoil. They surmised that effective separation control could be obtained by direct introduction of velocity disturbances. Bar-Sever[24] used a 0.1-mm tungsten wire to introduce transverse velocity fluctuations into a separated shear layer on an LRN(1)-1010 airfoil at high incidences. The wire was located 1.5 mm upstream and parallel to the airfoil's leading edge. The airfoil had a 15-cm chord and 30-cm span. The transverse oscillation of the wire was driven by an ac-current modulated horseshoe-shaped permanent magnet. At Reynolds number 1.5×10^5 forcing increased the maximum lift coefficient from 1.43 to 1.60, shifted the angle of attack from 11 to 20 deg, and moved the separation location from the leading edge

to about 80% chord length. A wide band of forcing frequencies (55–275 Hz) was found to be effective.

In this paper a passive self-excited, transversely oscillating-rod technique for the separation control of the boundary layer on a NACA 0012 wing model is developed and studied. The results show that improvements in the separation, stall angle of attack, and lift-to-drag ratio are remarkable.

Experimental Setup

The experiments were performed in a closed-return wind tunnel as shown in Fig. 1. The wind tunnel had a test section of 60 × 60 × 120 cm, made of one polished aluminum alloy plate as the floor and three high-transparency Plexiglas® panels as the ceiling and side walls for photography and visualization. The contraction ratio of the nozzle was 10 to 1. The stable operation velocity in the test section was between 0.7 and 60 m/s. The freestream turbulence intensity was less than 0.2% in the experimental range 5–45 m/s. The nonuniformity of the average velocity profile across the test section was lower than 0.5%. During the experiments, the average velocity of the approaching flow was determined with a pitot-static tube. An aluminum plate with sharp leading and trailing edges was placed 5 cm above the floor of the test section for control of the boundary-layer thickness. The experimental range of chord Reynolds number is 6×10^4–1.6×10^5.

The installation mechanism of wing model and control rod was shown in Fig. 2. The rectangular wing model with a NACA 0012 airfoil profile was made of stainless steel. The chord length and span are 6 and 30 cm, respectively, giving an aspect ratio 5. The wing model protruded vertically through the aluminum floor of the test section and the boundary-layer thickness control plate. The wing model was mounted on a JR^3 Universal Force-Moment System. The pivoting axis was located at one-fourth of the chord from leading edge. The assembly of wing model and balance was mounted on a rotary support. The JR^3 balance had a monolithic six-degree-of-freedom force sensor. The output electronic signals of the sensor were sampled by a PC-based high-speed data-acquisition system. The control rod was installed vertically on the chord plane at a distance l upstream and parallel to the leading edge of the wing model. The upper end of the rod was fixed on a circular disc with a screw nut. The circular disc was attached to a set of worm gears and in turn connected through the upper shaft, upper gear, chain, lower gear, lower shaft, and coupler to the shaft of the rotary mechanism. The lower end of the control rod was fixed on the flange of the rotary jig, so that the rod and the wing model can rotate simultaneously. The tightness (tension) of the rod could be adjusted via the screw nuts at two ends. The rod materials tested included iron, copper, and stainless steel. Rod diameter ϕ ranged from 1 to 4 mm. The distance l from the leading edge of the wing to the nearest rod surface was varied from 6 to 1 mm. Some selected small-diameter rods proceeded to a self-excited transverse vibration when they were placed very close to the leading edge. By adjusting rod tension via the screw nuts, the vibration frequency could be changed.

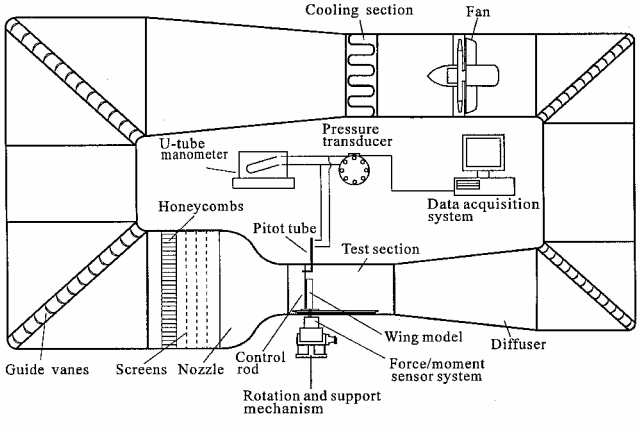

Fig. 1 Experimental setup.

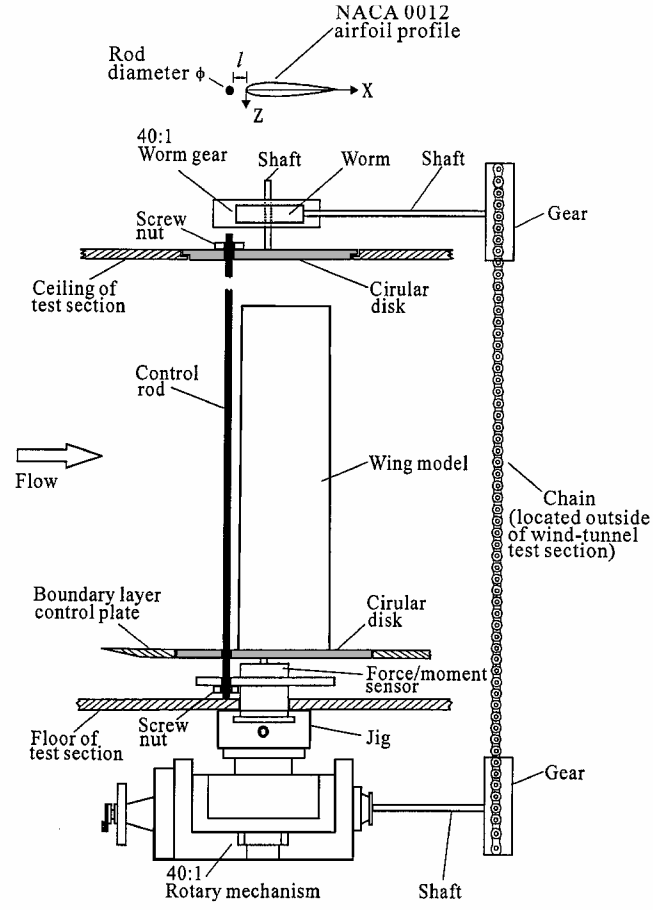

Fig. 2 Installation mechanism of wing model and control rod.

A diffusion-scan type Yamatake-Honeywell photoelectric switch was used to detect the vibration frequency and amplitude of the rod. The photoelectric switch consisted of a small-diameter optical fiber transmitter/receiver (model HPF-D018) and a high-response photoelectric amplifier (model HPX-F1). The 0.75-mm-diam transmitter/receiver produced a beam of modulated infrared light and received the target-reflected optical signals. Maximum sensing distance and minimum target size were 15 and 0.2 mm, respectively. The photoelectric amplifier had a frequency response limit of 20,000 Hz. The current outputs were shunt with a 1.2 kΩ resistor to convert into almost square-wave voltage signals. The voltage outputs were fed into a fast Fourier transform analyzer to extract the frequency information. The optical transmitter/receiver was connected to a precision stage through a L-shaped extension rod. Moving the photoelectric sensor across the vibration direction of the rod with the precision stage and recording the limiting positions where the square waves of output signals disappeared, the amplitude was obtained by subtracting the rod diameter from the measured distance between two limiting positions.

The surface oil-flow technique as described by Huang and Lin[25] was employed to detect the characteristics of flow modes. Mineral oil mixed with a small amount of blue dye powder was blush coated on the suction surface of wing model. Dark traces on the wing surface are located where the massive dyed-oil accumulated. The flow direction on the suction surface was observed in situ from the trace of oil-flow motion. The positions of separation and reattachment of boundary layer on the suction surface of the wing were taken from the recorded video images of the surface oil-flow patterns.

The accuracy of measurement of freestream velocity was affected primarily by the alignment of pitot tube and the calibration of pressure transducer. With the help of an on-line micropressure calibration system and careful alignment of pitot tube, the uncertainty in the freestream velocity was estimated to be no larger than ±1.5% of reading. The rotary support for the wing model had a resolution of 0.012 deg. The largest uncertainty in C_L is at near zero lift, that

is, at low angles of attack. It was estimated to be within ±1.5% of reading. The largest uncertainty in C_D appeared at zero angle of attack, where the drag was a minimum for about ±2.0% of reading. The accuracy of the vibration frequencies depends not only on the response of photoelectric amplifier but also on the record length and sampling rate of the FFT analyzer. The uncertainty of the frequency detection was estimated to be within ±0.75% of the reading in this experiment. The uncertainty of the vibration amplitude measurement was around ±5%.

Results and Discussion

Self-Excited Vibration Characteristics of Control Rod

Rods made of iron, copper, and steel with diameters ranged from 1 to 4 mm were tested. The distance l from leading edge of wing to the nearest rod surface was varied from 6 to 1 mm. A self-excited transverse vibration was observed when the small-diameter rods were placed very close (for example, 1 mm) to the leading edge. The self-excited vibration can be induced by the interaction between the elastic rod and the complex flows, which combine the jet through the gap between the rod and the leading edge of wing model, the wake behind the rod, and the boundary layer on the wing surface. The vibration frequency can be varied when the rod tension is changed via the screw nuts. For instance, the 1-mm iron rod placed at $l = 1$ mm can vibrate transversely at different "nominal"

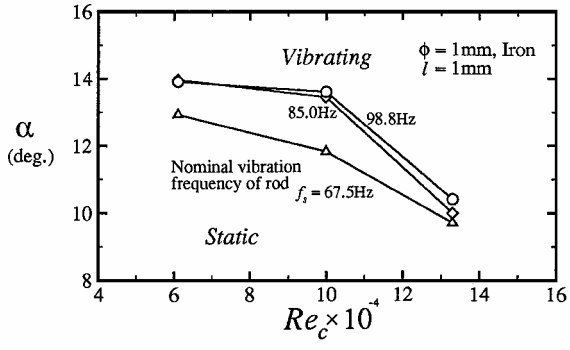

a) Domain of vibration

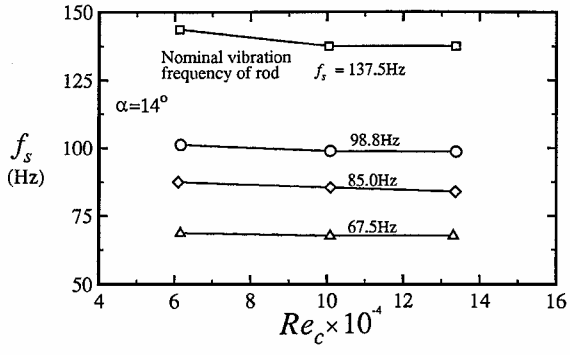

b) Effect of Reynolds number

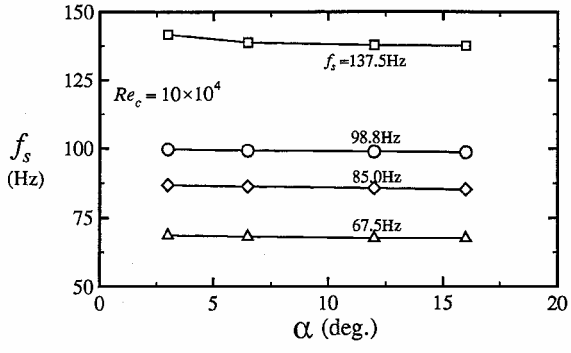

c) Effect of angle of attack

Fig. 3 Vibration frequency characteristics of control rod.

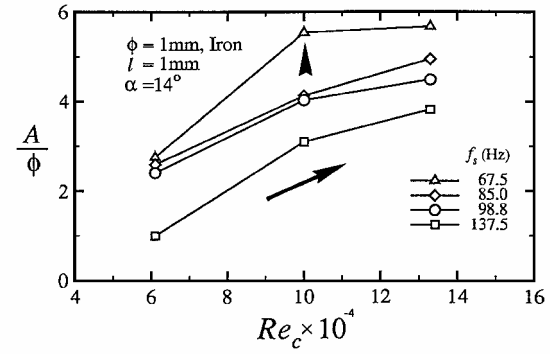

a) Effect of Reynolds number

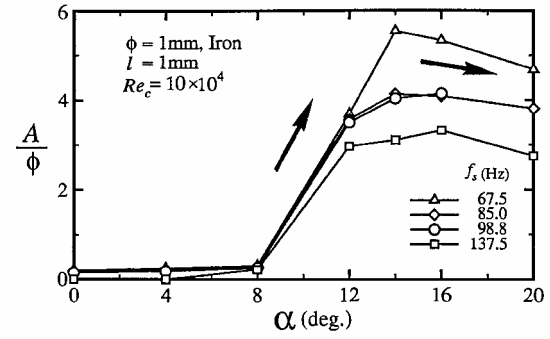

b) Effect of angle-of-attack

Fig. 4 Vibration amplitude characteristics of control rod.

frequency f_s if the Reynolds number and angle of attack are larger than the values located on the curves of Fig. 3a. In the lower left part of the curves, the rod remains static. The vibration frequency f_s is described as nominal because it decreases slightly with the increase of Reynolds number and angle of attack under a fixed tension, as shown in Figs. 3b and 3c. Because the variations are insignificant, the nominal vibration frequency is used hereafter.

In Fig. 4a the vibration amplitude increases with the increase of Reynolds number, but decreases with the increase of frequency. For example, at high frequency of 137.5 Hz the vibration amplitude is about three rod diameters smaller than that at 67.5 Hz. At $f_s = 67.5$ Hz it attains a large value of about 5.7 rod diameters at $Re_c \geq 10^5$. Resonance can occur at $f_s = 67.5$ Hz and $Re_c = 10^5$ because the vibration amplitude is abnormally large. The vibration amplitudes become remarkably large when the angle of attack is higher than about 8 deg, as shown in Fig. 4b. The vibration amplitudes attain maximum at $\alpha \approx 14$ deg, then decrease slowly with the increase of angle of attack. The stall angle of the NACA 0012 wing is about 10 deg. The control rod can set out a large vibration as $\alpha > 8$ deg, which makes a perfect match.

Surface Flow Patterns

The typical patterns of surface oil flow for the natural wing at $Re_c = 10^5$ are shown in Fig. 5. The corresponding hand sketches shown in Fig. 6 delineate the locations where massive dyed-oil accumulates and the in situ observed oil-flow directions. The bold lines delineate the separation or reattaching lines, whereas the thin lines with arrows indicate the paths and directions of the oil flow on the suction surface. The hand sketches at the bottom part delineate the side view of what is assumed to be the surface flow patterns in the two-dimensional area.

At $\alpha = 4$ deg, as shown in Figs. 5a and 6a, two dark lines appear. The left line is where the boundary layer separates, whereas the right one represents where the separated flow reattaches. Direction of the oil flow in the two-dimensional region shows the existence of a separation bubble between these two lines. The separation bubble moves toward the upstream area and becomes smaller with the increase of the angle of attack. At $\alpha = 8$ deg, as shown in Figs. 5b and 6b, the separation bubble becomes very small and is located very close to the leading edge. At $\alpha = 10$ deg, as shown in Figs. 5c and 6c,

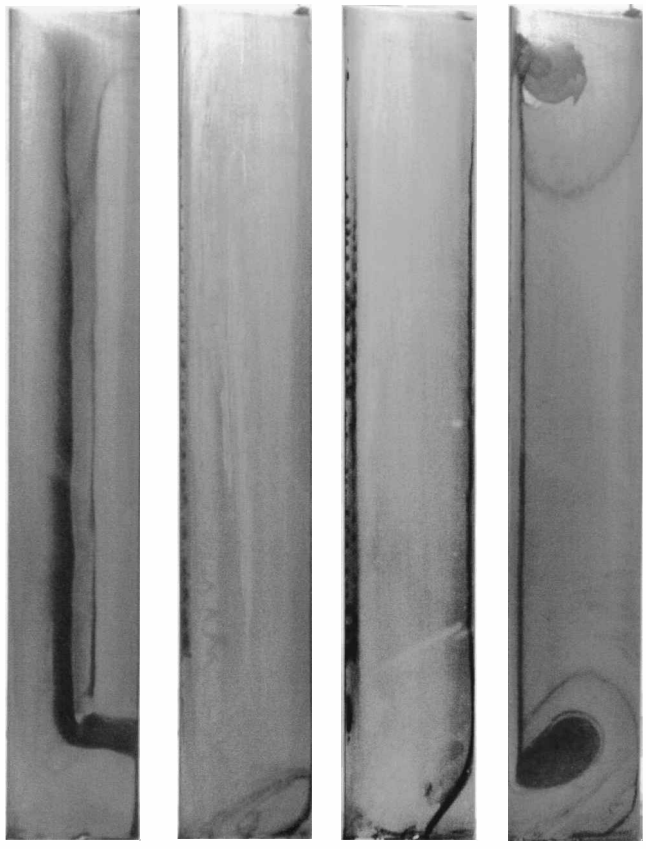

a) $\alpha = 4$ deg b) $\alpha = 8$ deg c) $\alpha = 10$ deg d) $\alpha = 12$ deg

Fig. 5 Typical surface oil-flow patterns on suction surface of natural wing at $Re_c = 10^5$.

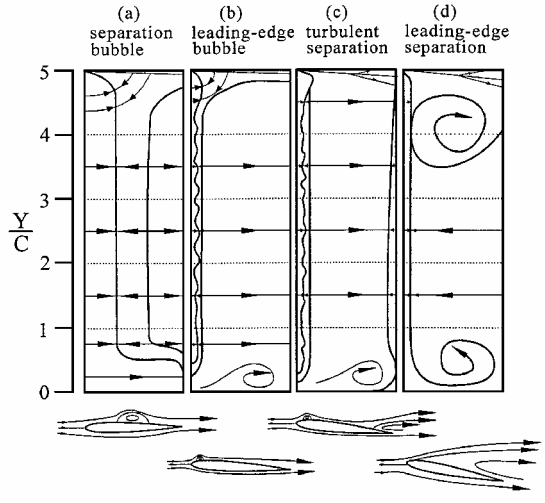

Fig. 6 Hand sketches of surface flow patterns corresponding to Fig. 5.

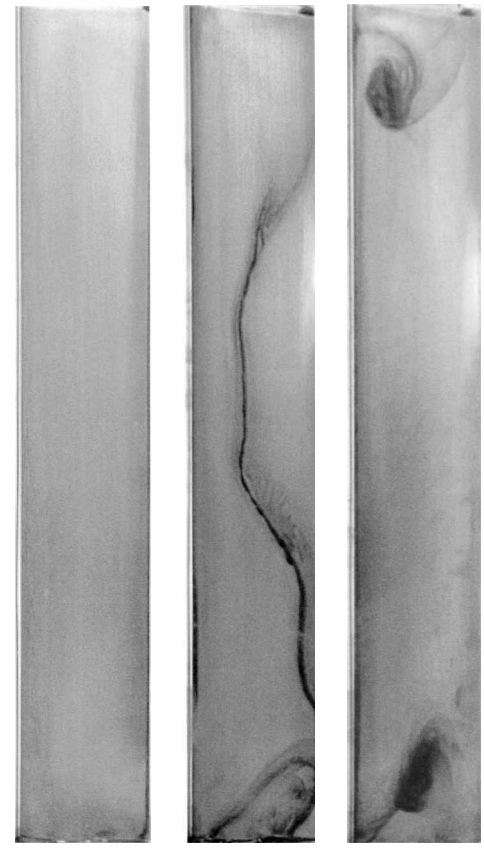

a) $\alpha = 3$ deg b) $\alpha = 13$ deg c) $\alpha = 20$ deg

Fig. 7 Typical surface oil-flow patterns on suction surface of vibrating rod-controlled wing at $Re_c = 10^5$.

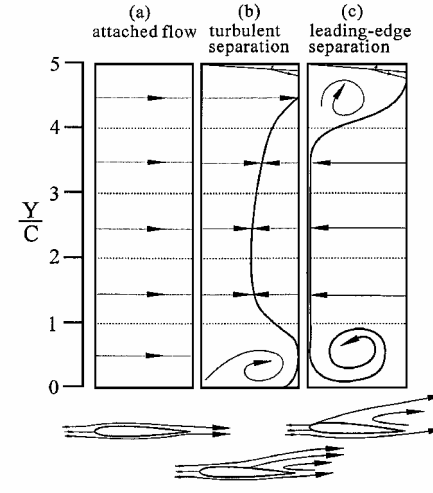

Fig. 8 Hand sketches of surface flow patterns corresponding to Fig. 7.

the reattached turbulent boundary layer separates and forms a separation line near the trailing edge. This separation line moves quickly toward the upstream as the angle of attack increases. At $\alpha = 12$ deg, as shown in Figs. 5d and 6d, the separation of the turbulent boundary layer occurs at the leading edge, accompanied by two large surface vortices[26] (one near the root area and the other near the wing tip). All of these surface oil-flow patterns are similar to those reported by Huang et al.[10] and Huang and Lee.[11]

When the wing model is subject to the influence of the vibrating rod, the surface flows are altered drastically, as shown in Figs. 7 and 8. The behavior of the surface flows becomes similar to the typical turbulent boundary layer,[3,12,27] that is, attached flows at low angles of attack (Figs. 7a and 8a), separation from trailing edge (Figs. 7b and 8b), and leading-edge separation (Figs. 7c and 8c).

Characteristic Flow Regimes

Figures 9a and 9b show the characteristic flow regimes of natural and vibration-controlled wings, respectively. It is obvious that the surface flows on the natural wing operated in the current experimental range of Reynolds numbers are characterized by the complex flow modes of laminar separation, separation bubble, leading-edge bubble, turbulent separation, and leading-edge separation. They are commonly observed at low Reynolds numbers 10^4–10^6 (Refs. 2, 3, 10, and 11).

As controlled by the vibrating rod, the turbulent boundary layer attaches to the wing surface at $\alpha \approx 7$ deg. As $\alpha > 7$ deg, the boundary layer starts to separate from the trailing edge. The separation line attains the leading edge at $\alpha \approx 18$ deg for $Re_c \geq 10^5$. For comparison, the case of rod-wake disturbed wing is shown in Fig. 9c. The distance

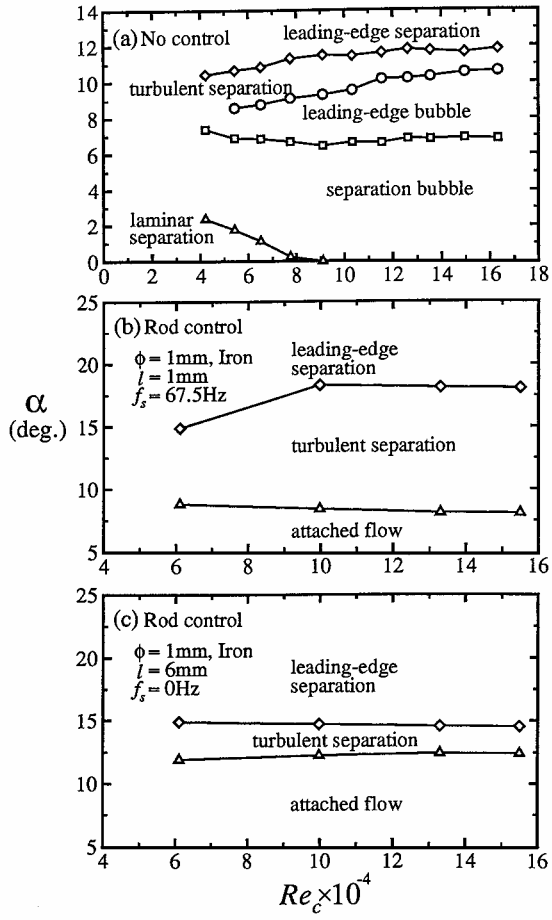

Fig. 9 Characteristic flow regimes: a) natural wing, b) vibrating rod-controlled wing, and c) rod-wake-disturbed wing.

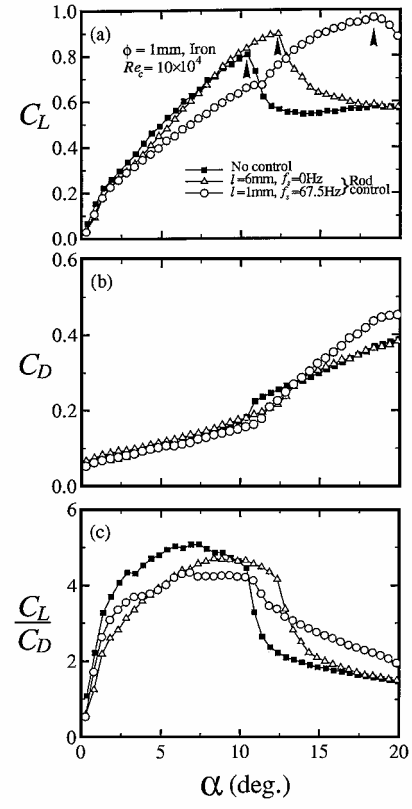

Fig. 10 Aerodynamic performance of natural, rod-wake-disturbed, and vibrating rod-controlled wings: a) lift coefficient, b) drag coefficient, and c) lift-to-drag ratio.

l between the rod and the leading edge is comparatively large (6 mm) so that the rod does not vibrate. Under the disturbance of the rod wake, the surface flows on the wing model also display typical characteristics of the turbulent boundary layer, which is similar to those shown in Fig. 9b. However, the characteristic modes cover different regimes. The boundary layer remains attached to the wing surface for $\alpha < 12$ deg. Once it separates, the separation line moves to the leading edge very fast when the angle of attack increases to about 15 deg.

In Figs. 9a and 9c the regimes of turbulent separation in common cover a narrow range (2–3 deg) of angle of attack. However, in the case of vibrating rod, as shown in Fig. 9b, separation starts at $\alpha \approx 7$ deg, then proceeds slowly toward the leading edge with the increase of angle of attack, finally attains the leading edge at $\alpha \approx 18$ deg, which is quite different from the natural and rod-wake disturbed wings. Apparently, the resistance to the separation is significantly improved when the wing is under the action of a vibrating rod. The boundary layer on the wing surface is drastically disturbed by transverse vibration of the rod. The boundary layer containing large turbulent kinetic energy as a result of the strong transverse velocity fluctuations can overcome moderate adverse pressure gradient[22,24] and defer the angle of attack at which the boundary layer separates from the leading edge.

Aerodynamic Performance

Natural, Rod-Wake Disturbed, and Vibrating-Rod Controlled Wings

Figure 10 shows the lift coefficient C_L, drag coefficient C_D, and lift-to-drag ratio C_L/C_D in three situations at $Re_c = 10^5$. As shown in Fig. 10a, C_L without control presents distinct slopes in different characteristic regimes of the surface flows, which are completely different from the conventional results[27] for Reynolds numbers larger than 10^6. The stall occurs at $\alpha \approx 10$ deg, where the boundary-layer separation occurs. When subject to the influence of rod wake without vibration, C_L increases without severe slope change, which is similar to the performance curve commonly observed in the high-Reynolds-number regime.[27] The stall is a little deferred to $\alpha \approx 12.5$ deg, where the turbulent boundary layer starts to separate. This value is very close to the stall angle 12.2 deg, which was measured by Abbott and von Doenhoff[27] at a high Reynolds number 6×10^6 for a standard roughness NACA 0012 airfoil. At stall, C_L decreases not so abruptly as the natural wing does. In the case of the vibrating rod, the lift coefficient before stall is lower than that of the natural wing. However, because of the large separation-resistance induced by strong transverse turbulence fluctuations the separation line of the turbulent boundary layer proceeds slowly to the leading edge with the increase of the angle of attack, as mentioned in Fig. 9b. The stall angle is deferred tremendously to $\alpha \approx 18$ deg, where the leading-edge separation occurs. It increases about 80% when compared with the natural wing. Maximum value of C_L is increased by about 20% from 0.8 of the natural wing to 0.97 in current case.

Variations of the drag coefficient C_D are shown in Fig. 10b. The drag generally increases with the increase of angle of attack. At stall, the slope of the drag curve increases appreciably as a result of the increase of the apparent form drag, which is induced by separation. The turbulent boundary layers create a large skin friction on the suction surface so that the drag coefficient in the case of turbulent surface flows is inevitably larger than that in the laminar case.

Before stall, the natural wing has larger lift-to-drag ratios than the rod-controlled ones, as shown in Fig. 10c, because the lift coefficients of the controlled cases are lower than that of the natural wing. At stall, C_L/C_D decreases drastically from 4.5 to 2 as a result of the abrupt loss of lift. After stall, the lift-to-drag ratios of the controlled ones are larger than that of the stalled natural wing. Particularly, the vibrating-rod controlled wing does not have an abrupt drop in C_L/C_D around the stall angle $\alpha \approx 18$ deg.

Effects of Reynolds Number

The variation of maximum C_L with Reynolds number is shown in Fig. 11a. Maximum lift coefficient of the natural wing increases

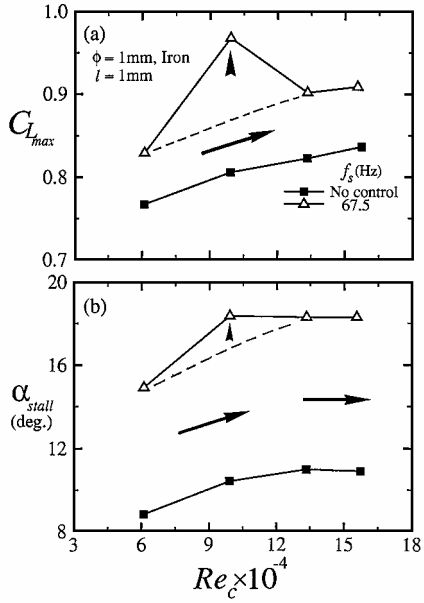

Fig. 11 Effects of Reynolds number on a) maximum lift coefficient and b) stall angle of attack.

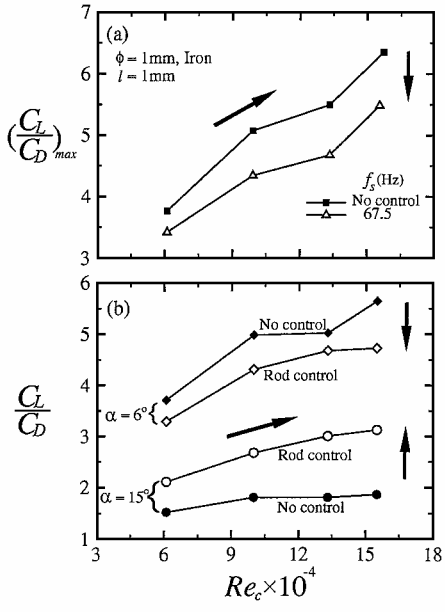

Fig. 12 Effects of Reynolds number on lift-to-drag ratio: a) maximum lift-to-drag ratio and b) comparison of lift-to-drag ratio before and after stall.

almost linearly with the increase of Reynolds number. Maximum C_L of the vibrating rod-controlled wing in general is about 0.1 larger than that of the natural wing, except at $Re_c = 10^5$, where a peak value 0.97 appears. Extraordinarily large vibration amplitude, as shown in Fig. 4a, possibly induced by resonance at this Reynolds number can cause such a high lift performance. The stall angle of attack of the vibrating rod-controlled wing is significantly improved by 6–8 deg when compared with that of the natural wing, as shown in Fig. 11b.

The maximum lift-to-drag ratio increases with the increase of Reynolds number for both the natural and vibration-controlled wings, as shown in Fig. 12a. The vibration-controlled wing has a lower maximum lift-to-drag ratio than the natural wing. Figure 12b shows the variation of the lift-to-drag ratios subject to the changes of the Reynolds number at low and high angles of attack. The lift-to-drag ratio generally increases with the increase of the Reynolds number. At low angle of attack, the vibration-controlled wing has

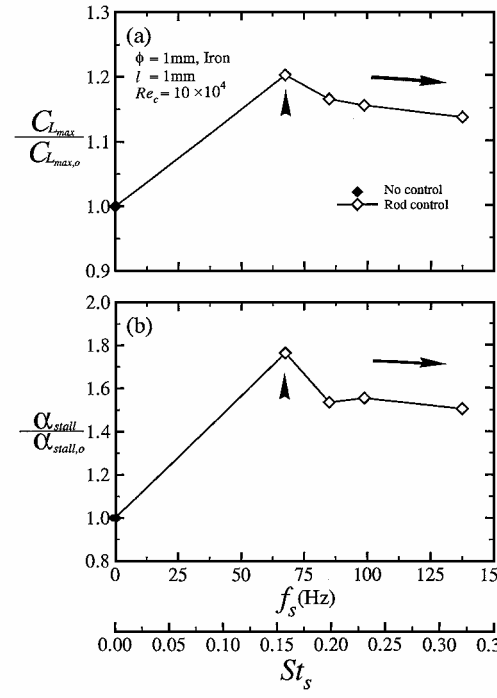

Fig. 13 Influences of vibration frequency on a) normalized maximum lift coefficient and b) normalized stall angle of attack.

lower lift-to-drag ratio than the natural wing. At large angle of attack, however, the situation is reversed.

Influences of Vibration Frequency

The influences of the vibration frequency on the normalized maximum lift coefficient at $Re_c = 10^5$ are shown in Fig. 13a. The normalization factor $C_{L\,\max,o}$ in the denominator is the maximum lift coefficient of the natural wing. At $f_s = 67.5$ Hz the normalized maximum lift coefficient increases to a maximum value 1.2, then decreases with the increase of frequency. The decrease rate becomes insignificant as the vibration frequencies are larger than 100 Hz. The influences of the vibration frequency on the stall angle of attack, as shown in Fig. 13b, behave similarly to those of the maximum lift coefficient. The normalized stall angle of attack increases to about 1.8, then decreases with the increase of vibration frequency. The influences become saturated at the vibration frequencies larger than about 100 Hz.

Conclusions

By installing a selected small-diameter metallic rod at a short distance ahead of the leading edge of a wing, a self-excited vibration of the rod can be induced. The natural, rod-wake disturbed, and vibrating rod-controlled wings show fundamental differences in the surface flow patterns and aerodynamic performance. The natural wing presents complex surface flow patterns, which are commonly observed at the Reynolds numbers between 10^4 and 10^6. Under the disturbances of the rod wake and rod vibration, the turbulent boundary-layer behaviors commonly found on a wing surface at large Reynolds numbers are obtained. The rod-wake disturbed boundary layer attaches to the wing surface without separation until an angle of attack is a little higher than the stall angle of attack of the natural wing. Once it separates, stall occurs, and the separation line moves to the leading edge with just a little increment of the angle of attack. The strong transverse velocity fluctuations induced by the vibrating rod make the boundary layer resistive to separation—the turbulent boundary layer separates slowly with the increase of the angle of attack. The stall occurs when the separation proceeds to the leading edge. The stall angle of attack can be deferred by about 80%. The maximum lift coefficient can be increased by about 20%. The Reynolds number as well as the vibration frequency and amplitude are determinants of the surface flows and aerodynamic performance.

References

[1]Carmichael, B. H., "Low Reynolds Number Airfoil Survey," Vol. 1, NASA CR 1165803, 1981.

[2]Lissaman, P. B. S., "Low Reynolds Number Airfoils," *Annual Review of Fluid Mechanics*, Vol. 15, 1983, pp. 223–239.

[3]Gad-el-Hak, M., "Control of Low-Speed Airfoil Aerodynamics," *AIAA Journal*, Vol. 28, No. 11, 1990, pp. 1537–1552.

[4]Crabtree, L. F., "Effect of Leading Edge Separation on Thin Wings in Two-Dimensional Incompressible Flow," *Journal of the Aeronautical Sciences*, Vol. 24, No. 8, 1957, pp. 597–604.

[5]Ward, J. R., "The Behavior and Effects of Laminar Separation Bubbles on Airfoils in Incompressible Flow," *Journal of the Royal Aeronautical Society*, Vol. 67, Dec. 1963, pp. 783–790.

[6]Arena, A. V., and Mueller, T. J., "Laminar Separation, Transition, and Turbulent Reattachment Near the Leading Edge of Airfoils," *AIAA Journal*, Vol. 18, No. 7, 1980, pp. 747–753.

[7]Mueller, T. J., and Batill, S. M., "Experimental Studies of Separation on a Two-Dimensional Airfoil at Low Reynolds Numbers," *AIAA Journal*, Vol. 20, No. 4, 1982, pp. 457–463.

[8]O'Meara, M. M., and Mueller, T. J., "Laminar Separation Bubble Characteristics on an Airfoil at Low Reynolds Numbers," *AIAA Journal*, Vol. 25, No. 8, 1987, pp. 1033–1041.

[9]Hsiao, F.-B., Liu, C.-F., and Tang, Z., "Aerodynamic Performance and Flow Structure Studies of a Low Reynolds Number Airfoil," *AIAA Journal*, Vol. 27, No. 2, 1989, pp. 129–137.

[10]Huang, R. F., Shy, W. W., Lin, S. W., and Hsiao, F.-B., "Influence of Surface Flow on Aerodynamic Loads of a Cantilever Wing," *AIAA Journal*, Vol. 34, No. 3, 1996, pp. 527–532.

[11]Huang, R. F., and Lee, H. W., "Effects of Freestream Turbulence on Wing-Surface Flow and Aerodynamic Performance," *AIAA Journal*, Vol. 36, No. 6, 1999, pp. 965–972.

[12]Gad-el-Hak, M., "Introduction to Flow Control," *Flow Control—Fundamentals and Practices*, edited by M. Gad-el-Hak, A. Pollard, and J.-P. Bonnet, Springer-Verlag, Berlin, 1998, pp. 1–153.

[13]Mangalam, S. M., Bar-Sever, A., Zaman, K. B. M. Q., and Harvey, W. D., "Transition and Separation Control on a Low-Reynolds Number Airfoil," *Proceedings of the International Conference on Aerodynamics at Low Reynolds Numbers*, Vol. I, Royal Aeronautical Society, London, 1986, pp. 10.1–10.19.

[14]Harvey, W. D., "Low-Reynolds Number Aerodynamics Research at NASA Langley Research Center," *proceedings of the International Conference on Aerodynamics at Low Reynolds Numbers*, Vol. II, Royal Aeronautical Society, London, 1986, pp. 19.1–19.49.

[15]Mueller, T. J., and Burns, T. F., "Experimental Studies of the Eppler 61 Airfoil at Low Reynolds Numbers," AIAA Paper 82-0345, 1982.

[16]Mehta, R. D., "Effect of a Longitudinal Vortex on a Separated Turbulent Boundary Layer," AIAA Paper 85-0530, 1985.

[17]Rao, D. M., and Kariya, T. T., "Boundary-Layer Submerged Vortex Generators for Separation Control—An Exploratory Study," AIAA Paper 88-3546-CP, 1988.

[18]Reynolds, W. C., and Carr, L. W., "Review of Unsteady, Driven, Separated Flows," AIAA Paper 85-0527, 1985.

[19]Schlichting, H., and Pechau, W., "Auftriebserhöhung von Tragflügeln Durch Kontinuierlich Verteilte Absaugung," *ZFW*, Vol. 7, 1959, pp. 113–119.

[20]Illingworth, C. R., "The Effect of Heat Transfer on the Separation of a Compressible Laminar Boundary Layer," *Quarterly Journal of Mechanical Applied Mathematics*, Vol. 7, 1954, pp. 8–34.

[21]Collins, F. G., and Zelenevitz, J., "Influence of Sound upon Separated Flow over Wings," *AIAA Journal*, Vol. 13, No. 3, 1975, pp. 408–410.

[22]Zaman, K. B. M. Q., Bar-Sever, A., and Mangalam, S. M., "Effect of Acoustic Excitation on the Flow over a Low Re Airfoil," *Journal of Fluid Mechanics*, Vol. 182, Sep. 1987, pp. 127–148.

[23]Chang, R. C., Hsiao, F. B., and Shyu, R. N., "Forcing Level Effects of Internal Acoustic Excitation on the Improvement of Airfoil Performance," *Journal of Aircraft*, Vol. 29, No. 5, 1992, pp. 823–829.

[24]Bar-Sever, A., "Separation Control on an Airfoil by Periodic Forcing," *AIAA Journal*, Vol. 27, No. 6, 1989, pp. 820, 821.

[25]Huang, R. F., and Lin, C. L., "Vortex Shedding and Shear-Layer Instability of Wing at Low-Reynolds Numbers," *AIAA Journal*, Vol. 33, No. 8, 1995, pp. 1398–1403.

[26]Bippes, H., "Experimental Investigation of Topological Structure in Three-Dimensional Separated Flow," *Proceedings of the IUTAM Symposium*, edited by F. T. Smith and S. N. Brown, Springer-Verlag, Berlin, 1987, pp. 379–381.

[27]Abbott, I. H., and von Doenhoff, A. E., *Theory of Wing Section*, Dover, New York, 1959, pp. 50–53.